Bending waves focusing in arbitrary shaped plate-like structures: Application to spatial audio in cars

Nassim Benbara*, Marc Rebillat, Nazih Mechbal

Processes and Engineering in Mechanics and Materials laboratory (PIMM) ENSAM, CNRS, CNAM, HESAM Université, 151 Boulevard de l'Hôpital, 75013 Paris, France

Keywords:
Spatial vibration control
Bending wave focusing
Multifunctional materials
Advanced signal processing
Inverse problems
Digital twin

A B S T R A C T

Advanced automotive audio applications are more and more demanding with respect to the visual impact of loudspeakers while still requiring more and more channels for high quality spatial sound rendering. The use of arbitrary plate-like structures driven by electromagnetic actuators or by piezoelectric elements appears as a promising solution to tackle both issues. However, to meet spatial rendering audio constraints (*i.e.* to be as close as possible to omnidirectional piston-like sources), the generated bending waves must be focused at a given position and to a certain extent within the host plate which can be of arbitrary shape, material, and thickness. Theoretically, this means being able to invert the spatio-temporal wave propagation operator for the generated bending waves to fit a given target shape. There are several methods (modal control, time-reversal, and propagating waves operator inversion) that allow to focus bending waves in a media. However, there is scarce work on their adaption and performances assessment in the context of audio applications. These methods depend differently on the available knowledge of wave propagation in the plate (theoretical, partial spatial or full spatial knowledge) and are here investigated to perform this task. Their performances are assessed with respect to several aspects: geometrical complexity, thickness, and material damping of the host structure, number and type of actuators, position and extent of the focusing area. The various methods are presented in a unified theoretical framework and they are compared by means of two key performance indexes (focus localization error and spatial contrast). An experimental validation on a relevant industrial case is also carried out and learning through a digital twin instead of time consuming experimental data investigated. This work falls within the framework of research which tries to bridge the gap between laboratory research and industrial deployment of this kind of technologies.

1. Introduction

Advanced automotive audio applications are more and more demanding with respect to the visual impact of loudspeakers while still requiring more and more channels for high quality spatial sound rendering. The main idea behind the concept of spatial sound rendering is to calibrate each loudspeaker of the array to reproduce with high fidelity the physics and the acoustics of the primary source [1]. Historically, spatial rendering methods such as stereophony (VBAP), binaural rendering

* Corresponding author.
E-mail address: nassim.benbara@ensam.eu (N. Benbara).

or holophony (ambisonic or Wave Field Synthesis (WFS)) have been achieved by means of electromagnetic loudspeakers. There are many constraints imposed by such methods for them to work properly: the setup must consist of several loudspeakers with a flat and omnidirectional response that are spatially evenly distributed to avoid spatial aliasing and able to cover the whole restitution area [2]. Distributed Mode Loudspeakers (DML) were introduced as a alternate to electrodynamical loudspeakers with a low visual profile [3]. The idea is to produce sound waves by exciting the bending waves of a thin stiff plate trough an actuator. This technology was used to render spatial sound by the WFS method [4,5]. However, this technology suffers from some drawbacks because of the aliasing caused by joint panels and the modal behaviour at low frequency of the plate which does not meet spatial audio requirements. Therefore, a new technology using larger plates called Multi-Actuator Panels (MAP) or much larger ones called Large Multi-Actuator Panels (LaMAP) has been designed to overcome these limitations [6]. This technology was successfully used in the context of WFS [7–9]. However, some drawbacks such as the modal behavior at low frequencies and the interferences between sources causing sound distortions and poor sound quality still exists with this technology.

Using spatial sound rendering coupled with flat panel loudspeaker appears as very interesting particularly in the automotive industry. Indeed, it will allow to alert directionally the driver from several dangers and to provide passengers with higher quality spatial sound. Moreover, this approach can potentially decrease weight by replacing electrodynamical loudspeakers with piezoelectric elements or audio exciters and improve design purposes and visual impact. However, inside a car, the rendering area is small and with very complex operational conditions (varying number of passengers, temperature variations, etc...). The classical methods (VBAP, Ambisonic, WFS) focus only on the targeted sound pressure field, which is a practical problem in cars because of the above mentioned very complex operational conditions. If one can control what happen on the vibrating surfaces instead of relying only on the emitted sound pressure, more robust sound rendering should be achieved. Considering the previous observations, focusing bending waves on arbitrary plate-like interior parts of the car to create independent sound sources appears as a promising way to create an array of audio sources that can be used in a second time for spatial sound rendering for automotive applications. Nevertheless, car interior surfaces are far from the simple rectangular homogeneous flat plates used when designing DMLs, MAPs and LaMAPs. As a consequence, several additional aspects must be considered in that context: the geometrical complexity, thickness, and material damping of the host structure, the number and location of actuators, and finally the position and extent of the focusing area.

In the literature, there are various methods that allow to focus bending waves in a media. The first method called modal control (MC) is based on modal superposition [10]. It allows focusing a monochromatic vibro-tactile peak on plates [11,12], or an audio source on a rectangular plate by computing FIR filters of order 3 [13]. The method is based on a simple approach (model-based) and is extremely sensitive to modeling error. The second method available in the literature is based on the time reversal (TR) principle, initially described by Fink et al. in [14]. It allows to focus a wave at a specific point in the space by learning partially the waves received at the actuators positions and initiated at the focusing point. Besides, the same author shows that this method can be adapted for acoustic purposes to control precisely acoustic wave propagation in reverberating cavities or in waveguides [15]. Additionally, this method is also used in [16] to focus an audio impulse in a room. Finally, the ease of the implementation of the time reversal encouraged many researchers to use it in haptic feedback applications [17]. The third method studied in this paper is the spatio-temporal inverse filtering (STIF), initially studied by Kahana et al. [18] and Tanter et al. [19] to find a solution to the lack of robustness of the time reversal method. Firstly, the method consists in learning the propagation of the waves in the whole media, then, an inverse filter is created and used as input for each actuator. Then, the method was extended to the time domain [20], and after experimentally applied in heterogeneous, absorbing and highly reverberating medias such as a human skull [21], or to focus acoustic waves in rooms [22]. Finally, the inverse filtering is also used in [23] using two different approaches to radiate a uniform sound field with a plate actuated by exciters at the periphery, creating a radiating zone in the middle of the plate. And in [24], the same authors use the inverse method to create a piston on a vehicle's roof for a narrow bass frequency band. Here, the purpose of this study is to try to bridge the gap between laboratory research and industrial deployment of the LaMAPs. Hence we propose here to work on the structural control of bending waves on a large frequency band, by comparing three rendering methods, according to several parameters.

Consequently, the objectives of this study are:

1. to adapt to audio applications the previously mentioned methods for the localization of bending waves in a defined area of a geometrically complex structure with arbitrary boundary conditions,
2. to assess their performances with respect to several aspects: geometrical complexity, thickness, and material damping of the host structure, number and type of actuators, position and extent of the focusing area.

The specific requirements for these methods in the present context are that they should be precise in terms of spatial focusing and must operate in a wide frequency range to be suitable for the audio restitution. Besides, the methods used should also be as insensitive as possible to noise and model error. Their performances are thus compared by means of two key performance indexes (focus localization error and spatial contrast). Finally, the methods should not rely on too much experimental measurement for practical reasons as the automotive industry is targeted as the applicative field. These adapted methods will first be presented in a unified formalism and then compared numerically to highlight the advantages and drawbacks of each method before comparing them experimentally on a realistic industrial case.

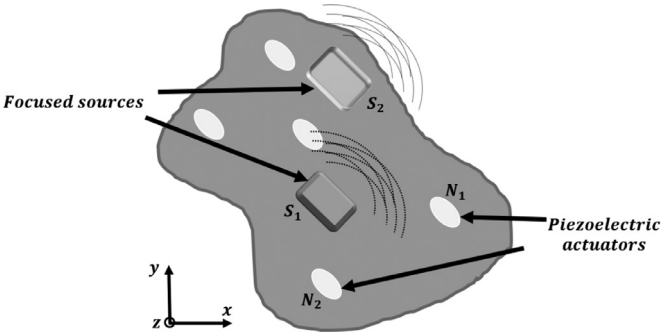

Fig. 1. Arbitrary shaped-like structure with piezoelectric actuators and localized audio sources.

2. Problem statement

Let S denote a plate-like structure of arbitrary shape and with arbitrary boundary conditions. Assuming that this structure lies in the (x, y) plane, the positions of the N actuators (piezoelectric or audio exciter) bonded on S are given by $\{(x_n, y_n)\}_{n \in [1,N]}$ and the out-of-plane displacement of the bending wave velocity field is denoted $u(x, y, t)$ (Fig. 1).

The objective is now, for any input audio signal $a(t)$, to focus the bending wave field $u(x, y, t)$ to fit a given target shape $\phi(x, y)$ using the N actuators through N FIR filters $r_n(t)$ applied to the audio input. Mathematically, this means that we would like to achieve:

$$\forall t \; u(x, y, t) = \phi(x, y)a(t). \tag{1}$$

Or equivalently in the frequency domain, with $U(x, y, f)$ and $A(f)$ the Fourier transforms of the displacement and the audio signal respectively:

$$\forall f \; U(x, y, f) = \phi(x, y)A(f). \tag{2}$$

Assuming the system is globally linear (the path between an actuator and a sensor is considered as linear), the contributions $u_n(x, y, t)$ of all the N actuators generating the field $u(x, y, t)$ sum up and can be written as:

$$\forall t \; u(x, y, t) = \sum_{n=1}^{N} u_n(x, y, t) = \sum_{n=1}^{N} h_n(x, y, t) * r_n(t) * a(t), \tag{3}$$

where "$*$" stands for the convolution product and $h_n(x, y, t)$ is the spatio-temporal impulse response of the nth actuator. Or equivalently in the frequency domain:

$$\forall f \; U(x, y, f) = \sum_{n=1}^{N} U_n(x, y, f) = \sum_{n=1}^{N} H_n(x, y, f)R_n(f)A(f). \tag{4}$$

By combining both expressions (2) and (4) of $U(x, y, f)$, the objective to achieve is then expressed in the frequency domain independently of the input signal $a(t)$ as:

$$\text{Find}\{R_n(f)\}_{n\in[1,N]}\text{such that}\forall f, \phi(x, y) = \sum_{n=1}^{N} H_n(x, y, f)R_n(f). \tag{5}$$

This means that the spatio-temporal propagation operators $H_n(x, y, f)$ associated with the N actuators needs to be inverted to design the N FIR filters $R_n(f)$ able to focus the bending wave field on the target shape $\phi(x, y)$ whatever the frequencies f contained within the input audio signal $a(t)$. In practice, focusing the bending waves thus consists in finding for each frequency the adequate phases and amplitudes to drive coherently each actuator bonded on the structure.

3. Bending waves focusing methods unified theoretical description

In this section, several methods able to invert the spatiotemporal propagation operator $H_n(x, y, f)$ are presented. The methods differ depending on the available knowledge of wave propagation in the plate they rely on. Indeed, the first method relies on theoretical knowledge and is named Modal Control (MC), the second method relies on partial spatial knowledge and is referred as Time Reversal (TR), and the last one is based on a full spatial knowledge and is named Spatio-Temporal Inverse Filter (STIF). They are all presented within a unified theoretical framework for comparison purpose.

The first class of methods presented here assumes that a theoretical knowledge of wave propagation within the host structure is known. For bending waves, the out-of-plane displacement $u(x, y, t)$ of the host structure (here a rectangular uniform plate) subject to the external load $p(x, y, t)$ can be expressed as [33]:

$$D\nabla^4 u(x,y,t) + \rho h\ddot{u}(x,y,t) + c\dot{u}(x,y,t) = p(x,y,t) \quad \text{with} \quad D = \frac{Eh^3}{12(1-\nu^2)}. \tag{6}$$

In the above equations, E, ν, and ρ are the Young's modulus, Poisson's ratio, and density of the panel respectively. Additionally, c is the damping constant and h is the panel thickness.

Let $\theta_m(x, y)$ be the theoretical orthogonal modes associated with the structure under study which can be computed analytically or through FEM models. The displacement can be written as a decomposition in the mode shape basis:

$$u(x,y,t) = \sum_{m=1}^{\infty} u_m(t)\theta_m(x,y), \tag{7}$$

where the coefficients $u_m(t)$ denote the modal amplitudes. By reinjecting the displacement expression (7) in the movement Eq. (6), and by projecting the obtained equation on the M first modes, the orthogonality property allows to get the decoupled equation for each modal displacement $u_m(t)$:

$$\forall m \in [1, M], \ddot{u}_m(t) + c\dot{u}_m(t) + (2\pi f_m)^2 u_m(t) = \frac{1}{S_m} p_m(x,y,t) \quad \text{with} \quad f_m = \frac{1}{2\pi}\sqrt{\frac{D}{\rho h}}k_m^2. \tag{8}$$

In the above equation, f_m is the eigen frequency corresponding to the mth mode and k_m^2 the wave number depending on the geometry. Additionally, S_m is the projection term and $p_m(x, y, t)$ the modal force given by:

$$S_m = \iint_S \rho h \theta_m(x,y)^2 \mathrm{d}x\mathrm{d}y \quad \text{and} \quad p_m(x,y,t) = \iint_S p(x,y,t)\theta_m(x,y)\mathrm{d}x\mathrm{d}y. \tag{9}$$

We can then write in the frequency domain, at the nth actuator:

$$\forall m \in [1, M], \forall f, U_{n,m}(f) = \frac{1}{S_m((2\pi f_m)^2 + (\mathrm{i}2\pi f)c + (\mathrm{i}2\pi f)^2)} P_{n,m}(x, y, f). \tag{10}$$

In case of no punctual actuation (where the area is denoted S_{act}), the modal force is given by :

$$P_{n,m}(x,y,f) = \left[\iint_{S_{act}} b_n(x,y)\theta_m(x_n,y_n)\mathrm{d}x\mathrm{d}y\right] R_n(f)A(f) = B_{n,m}R_n(f)A(f), \tag{11}$$

where $b_n(x, y)$ is a shape function characterizing the spatial distribution of each actuator.

Finally, by summing over all modes and actuators, one obtains:

$$\begin{aligned} \forall f, \ U(x,y,f) &= \sum_{n=1}^{N}\left[\sum_{m=1}^{M} \frac{B_{n,m}\theta_m(x,y)}{S_m((2\pi f_m)^2 + (\mathrm{i}2\pi f)c + (\mathrm{i}2\pi f)^2)}\right] R_n(f)A(f) \\ &= \sum_{n=1}^{N} H_n(x,y,f)R_n(f)A(f). \end{aligned} \tag{12}$$

This constitutes a theoretical expression of the spatio-temporal bending wave propagation operator $H_n(x, y, f)$ that needs to be inverted.

Now, by decomposing the target $\phi(x, y)$ on the host structure mode shapes $\theta_m(x, y)$ as:

$$\phi(x,y) = \sum_{m}^{M} \phi_m\theta_m(x,y) \ \ with \ \ \phi_m = \iint_S \phi(x,y)\theta_m(x,y)\mathrm{d}x\mathrm{d}y. \tag{13}$$

We can write the following equation after projecting on each mode ϕ_m:

$$\forall f, \forall m \ \ \phi_m = \sum_{n}^{N}\left[\frac{B_{n,m}\iint_S \theta_m(x,y)\mathrm{d}x\mathrm{d}y}{S_m\left((2\pi f_m)^2 + (\mathrm{i}2\pi f)c + (\mathrm{i}2\pi f)^2\right)}\right] R_n(f). \tag{14}$$

with the number of modes M chosen equal to the number of actuators or superior (potential matrix conditioning problem during the inversion). The previous equation can be written in the matrix form as $\mathbf{\Phi} = \mathbf{H}(x, y, f)\mathbf{R}(f)$. When inverting $\mathbf{H}(x, y, f)$, it gives:

$$R_n(f) = \left[\frac{\mathbf{B_m^{-1}}}{\left(\iint_S \theta_m(x,y)\mathrm{d}x\mathrm{d}y\right)}\right]\left[S_m\left((2\pi f_m)^2 + (\mathrm{i}2\pi f)c + (\mathrm{i}2\pi f)^2\right)\right]\phi_{\mathbf{m}}, \tag{15}$$

where $\mathbf{B_m}^{-1}$ represent the mth line of the inverted matrix $\mathbf{B^{-1}}$. Going back to the time domain, it can be shown [13] that such equation can be expressed in the discrete-time domain as follows:

$$R_n(z) = J_n + K_n z^{-1} + L_n z^{-2}. \tag{16}$$

Where J_n, K_n and L_n can be expressed using the modal parameters (k_m, $\boldsymbol{\theta}_{\mathbf{m}}(x_n, y_n)$) as well as the target shape parameters $\boldsymbol{\phi}_{\mathbf{m}}$.

The method described above offers the advantage of not needing any prior experiments. Indeed, only the analytical knowledge of the model is needed. In addition, the computation cost is low because the FIR filter order is 3 and the method is not sensitive to noise, because no prior measures are done. Finally, the method allows to reproduce arbitrary target shapes. However, the advantages listed before are available only for very simple structures. Indeed, only simple structures such as rectangular or circular plates with boundary conditions known analytically can be used. Additionally, for an audio purpose the frequency bandwidth is in general large and the number of modes to be addressed might be high. However, the theory assumes that the number of modes controlled is equal to or a bit higher than the number of actuators so that the matrix can be inverted, or pseudo-inverted and matrix conditioning issues can be avoided, but it will not be the case practically.

3.2. Methods relying on a partial spatial knowledge of $\mathrm{H_n(x, y, f)}$

Let us now assume that a partial spatial knowledge of the propagation operator is available. More precisely, it is assumed here that the spatio-temporal operator is known for an excitation located at one spatial position (x_i, y_i) and measurements performed at actuator positions $\{(x_n, y_n)\}_{n \in [1,N]}$. This propagation operator impulse response is denoted $\left\{\widehat{h}(x_n, y_n, t)\right\}_{n\in[1:N]}$. Moreover, the measured impulse response between the actuator n and the receiving point at the position (x_i, y_i) in the time domain is $h_n(x_i, y_i, t)$ such that:

$$\forall n \in [1, N]\ \hat{h}(x_n, y_n, t) = h_n(x_i, y_i, t). \tag{17}$$

According to the spatial reciprocity principle [15], the FIR filters are chosen by reversing the time, *i.e.* by applying the transformation $t \longmapsto -t$:

$$\forall n \in [1, N]\ r_n(t) = \hat{h}(x_n, y_n, -t). \tag{18}$$

In the frequency domain, by taking the Fourier transform of $r_n(t)$, one obtains:

$$\begin{aligned} R_n(f) &= \int_{-\infty}^{+\infty} \widehat{h}(x_n, y_n, -t)\mathrm{e}^{-\mathrm{i}2\pi ft}\mathrm{d}t \underset{u=-t}{=} \int_{-\infty}^{+\infty} \widehat{h}(x_n, y_n, u)\mathrm{e}^{\mathrm{i}2\pi fu}\mathrm{d}u \\ &= \mathrm{conj}\left[\int_{-\infty}^{+\infty} \widehat{h}(x_n, y_n, u)\mathrm{e}^{-\mathrm{i}2\pi fu}\mathrm{d}u\right] = \mathrm{conj}[\widehat{H}(x_n, y_n, f)]. \end{aligned} \tag{19}$$

Through this procedure, one should be able to focus the bending waves in the neighborhood of the location (x_i, y_i). Using previous notation, this means that the target shape to be reconstructed corresponds here to a Dirac function located at (x_i, y_i), *i.e.*, $\phi(x, y) = \delta(x - x_i, y - y_i)$.

According to the theory, this method is based on the time invariance principle of partial derivative equations in an undamped media. Indeed, if a structure is excited at a point A and the wave measured at the point B, therefore the excitation at B and measurement at A gives the same response function. Even if the invariance ensure the filters robustness, the approximation in thin and low damped structure is made. The method furthermore needs to be extended to a wider target shape by considering time reversal on adjacent points because for the moment there is no control of the width. Finally, the computation cost must be discussed. Theoretically, impulse responses must be measured between each focus point and actuator. If the position of the focus area location is known, the number of initial measurements will be very low. The method may also be sensitive to the experimental noise.

3.3. Methods relying on a complete spatial knowledge of $\mathrm{H_n(x, y, f)}$

Let us now assume that a complete spatial knowledge of the propagation operator is available. More precisely, it is assumed here that the spatio-temporal operator is known for any actuator $n \in [1, N]$ and that measurements are performed over a complete grid of K points on the structure for positions $\{(x_k, y_k)\}_{k \in [1,K]}$. Mathematically, what is known in the frequency domain is $\{H_n(x_k, y_k, f)\}_{n \in [1:N], k \in [1,K]}$.

The problem to be solved can then be rewritten on the measurement spatial grid as:

$$\phi(x_k, y_k) = \sum_{n=1}^{N} H_n(x_k, y_k, f)R_n(f). \tag{20}$$

Thus, in the matrix form:

$$\Phi = \mathbf{H}(f)\mathbf{R}(f). \tag{21}$$

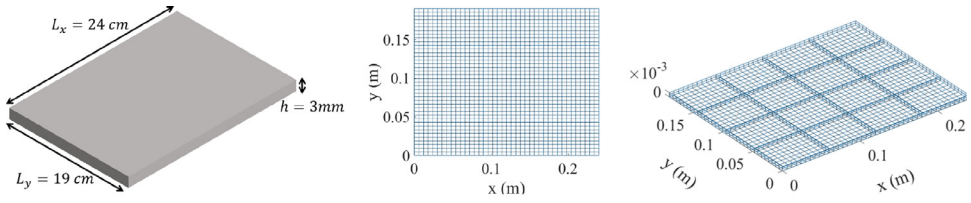

(a) (b) (c)

Fig. 2. (a) Dimensions of the plate and (b) meshes of the studied plate and (c) ribbed plate.

Table 1
First eigen frequencies and damping ratios of the plate.

Index	Eigen frequency (Hz)	Damping (%)
Mode (1,1)	127	4.2
Mode (2,1)	222	4,7
Mode (1,2)	292	3.8
Mode (2,2)	379.4	2.1
Mode (3,1)	379.9	2,1
Mode (3,2)	530	3

The resulting matrix can first be directly pseudo-inversed in the frequency range of interest by keeping only large enough eigenvalues. This leads directly to the FIR filters $R_n(f)$:

$$\mathbf{R}(f) = \mathbf{H}(f)^{+}\Phi, \tag{22}$$

where "+" denotes the pseudo-inversion operator.

It is important to note that the pseudo-inversion step is sensitive to noise. Hence, during the pseudo-inversion step, the lowest singular values are canceled to deal with those matrix conditioning issues. More details are available in [21].

This method offers several advantages in comparison with the others evoked previously. Firstly, the method is robust because it allows acquiring information about the wave propagation in the whole media. Additionally, the filter size is chosen by the user. Hence, the model takes into account the real structure and its complexity, with eventual losses, and the notion of modal density is not crucial. Finally, this method is very interesting for its ease of implementation. Nevertheless, the points evoked above are also sources of drawbacks. Indeed, it is necessary to realize several experiments between all the points of the structure and the actuators, this complicates numerically the method. Moreover, the method is sensitive to the noise, mainly during the pseudo-inversion step. Thus, it could need a regularization step which is numerically heavy.

4. Numerical study of the investigated focusing methods

4.1. Structures under study

In order to test the previous methods and to compare their performances, a simple and a ribbed clamped plate are chosen. Polypropylene is selected here as it is a material often used for car passenger garnishments. The dimensions of the plate are given in Fig. 2a. Besides, ribs with length of 1 cm and thickness of 3 mm are added to approach as much as possible the surfaces used in the automotive industry. The ribs are stiffening the plate, shifting the eigenmodes to higher frequencies and introducing localized modes.

The material used is polypropylene, with a Young modulus of $E = 1.1$ GPa, a Poisson's ratio of $\nu = 0.33$ and a density of $\rho = 990$ kg/m^3. Mode shapes of the structures are computed thanks to a finite element model implemented on the software SDT (SDTools©, Structural Dynamics Toolbox [25]) and an experimental modal analysis was performed jointly to identify modal dampings, available in Table 1. The modal identification was achieved by using a sine sweep input signal. After the transfer functions have been acquired thanks to a piezoelectric actuator and a laser Doppler vibrometer sensor, a pole/residue parametrization was made to identify the modal characteristics of interest (the test rig is described precisely in Section 5.1). The studied plate is relatively damped and therefore different from the most frequently handled cases in the literature which involve very low damped structures such as metal plates or smartphone glasses [12,13,17].

The plate is modeled with shell elements. The bending wave focusing algorithms are developed and implemented in Matlab with SDT software jointly. The meshes are available Fig. 2b and c. Throughout the remaining of this study, the audio signal to be reconstructed is a sweep sine with a duration of 2 s, spanning frequencies from 100 Hz to 800 Hz, sampled at 44.1 kHz. The chosen frequency range allows to excite the 6 first modes

In the following sections, there will first be a parametric study aimed at comparing the three methods theoretically studied previously (Section 3) by varying several parameters. The parameters to be studied are :

- the damping ratio and the thickness, because the car door panel material is made up of polypropylene, with variable thickness and coating,
- the number of actuators, because only a small number of exciters can be integrated for reason of compactness,
- the geometric complexity (ribbed plate versus simple plate),
- the position and the size of the target shape.

The three methods described previously are applied numerically, and compared to a case where no control is imposed (no control), that consists in actuating only the nearest actuator to the target shape.

4.2. Key performance indicators for the parametric study

Four original key performance indicators will be used in order to compare the 3 methods previously presented when varying damping, the number of actuators and the geometrical complexity on the structure under study. These indicators are described below. Keep in mind that $u(x, y, t)$ is the out-of-plane displacement of the plate and $U(x, y, f)$ its Fourier transform.

Localization error: given a reconstructed target shape, the first criterion is the measurement between the center of the target shape and the maximum amplitude of the reconstructed shape. Thus, the lower the distance is, the more the shape is localized precisely from a spatial point of view.

Spatial contrast: the second criterion is the computation of the contrast between the energy in the reconstructed area (S_R) and energy of the total area ($S_T = L_x \times L_y$), so that:

$$C(f) = \frac{\iint_{S_R} |U(x, y, f)|^2 \mathrm{d}S}{\iint_{S_T} |U(x, y, f)|^2 \mathrm{d}S}. \tag{23}$$

If $C(f) = 1$, then all the energy is present in the target shape and nothing outside, and if $C(f) = 0$, then all the energy is outside the target shape.

Normalized mean quadratic displacement: the normalized mean quadratic displacement amplitude of bending waves in the frequency range of interest is defined by:

$$< |U(x, y)|^2 >= \frac{1}{f_{\max} - f_{\min}} \int_{f_{\min}}^{f_{\max}} |U(x, y, f)|^2 \mathrm{d}f, \tag{24}$$

It provides a visual overview of how well the algorithms are able to focus bending waves in the targeted frequency range.

Mean quadratic phase variation: this KPI corresponds to the average quadratic phase difference between the point $(x_{\max}, y_{\max})$ at which the maximum of the amplitude is reached and the current point (x, y):

$$\Phi(x, y) = \frac{1}{f_{\max} - f_{\min}} \int_{f_{\min}}^{f_{\max}} \mathrm{phase}\left[\frac{U(x, y, f)}{U(x_{\max}, y_{\max}, f)}\right]^2 \mathrm{d}f. \tag{25}$$

It provides a visual overview of how well the algorithms are able to focus bending waves with spatially coherent phase in the targeted frequency range.

4.3. Parametric study for the bending wave focusing

4.3.1. Influence of damping and thickness of the plate

The case that is considered is with an actuator configuration (3×2), a size shape of ($0.25L_x$, $0.3L_y$) and a target shape position centered at ($0.3L_x$, $0.6L_y$), as shown in Fig. 4d. The Fig. 3 shows the contrast (Fig. 3a, c, e) and spot error (Fig. 3b, d, f) of the three algorithms and for the case without any control (Fig. 3g, h) according to simultaneously damping variations (from 1% to 6%) and thickness variations (from 1 mm to 5 mm). It can be seen that the STIF method localizes waves always very efficiently (high contrast and low spot error), and far better with high thicknesses. For low level of thickness, the contrast increases with damping, but after 3 mm, the damping has less effects than thickness. Conversely, the TR method contrast is higher and spot error lower with low thickness (1 mm to 2 mm). Above this value of thickness, the ability to focus is poorer. For these two thicknesses, the performance increases with damping. For the MC, the contrast increases from 0.4 to 0.7 with the damping ratio. For the no control case, the plate behaves according to its modal shapes, so that the contrast is always around 0.4 and the spot error varies randomly. According to these curves, the STIF is performing much better than the no control case, the MC is better for higher damping and thickness, and the TR for thinner plates.

4.3.2. Effect of actuator disposition and thickness

This subsection aims to study the effect of the number of actuators for several thicknesses. Having more actuators could be interesting because one can control only as many modes as the number of actuators in the modal control context. However, in the perspective of applying these methods to real systems, an optimization of the number of active elements is necessary. The Fig. 4 shows the selected dispositions of the actuators, which are evenly spaced along x and y. The Fig. 5 shows the contrast and spot error for the three methods according to the thickness and for the all the chosen configurations.

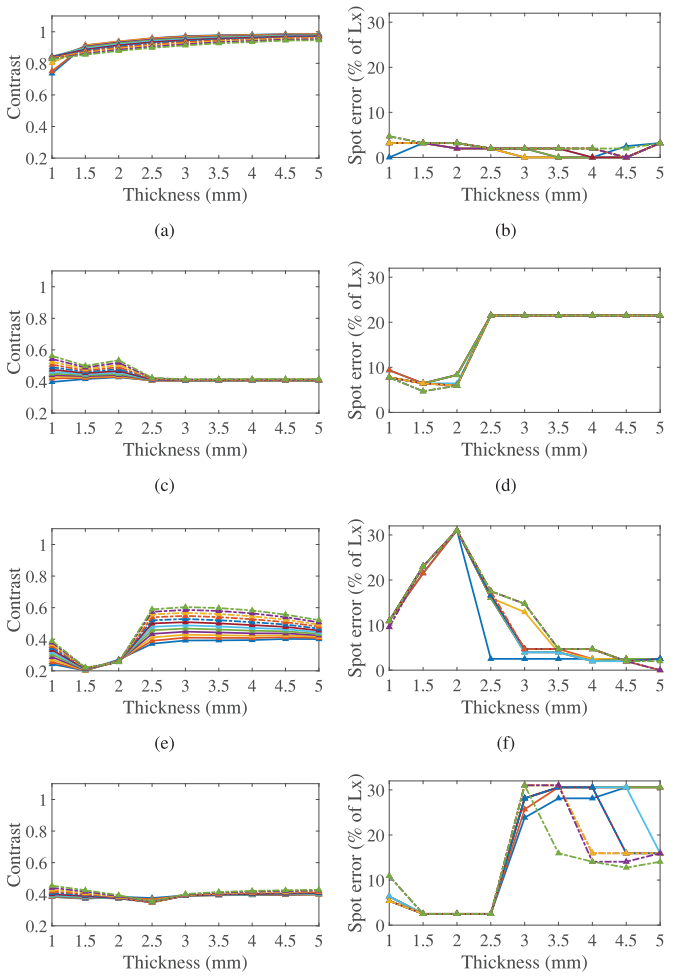

Fig. 3. Contrast and spot error ((a)(b) STIF, (c)(d) TR, (e)(f) MC, and (g)(h) No control) according to the damping: (1%) (1.5%) (2%) (2.4%) (2.8%) (3.3%) (3.7%) (4.2%) (4.6%) (5%) (5.5%) (6%).

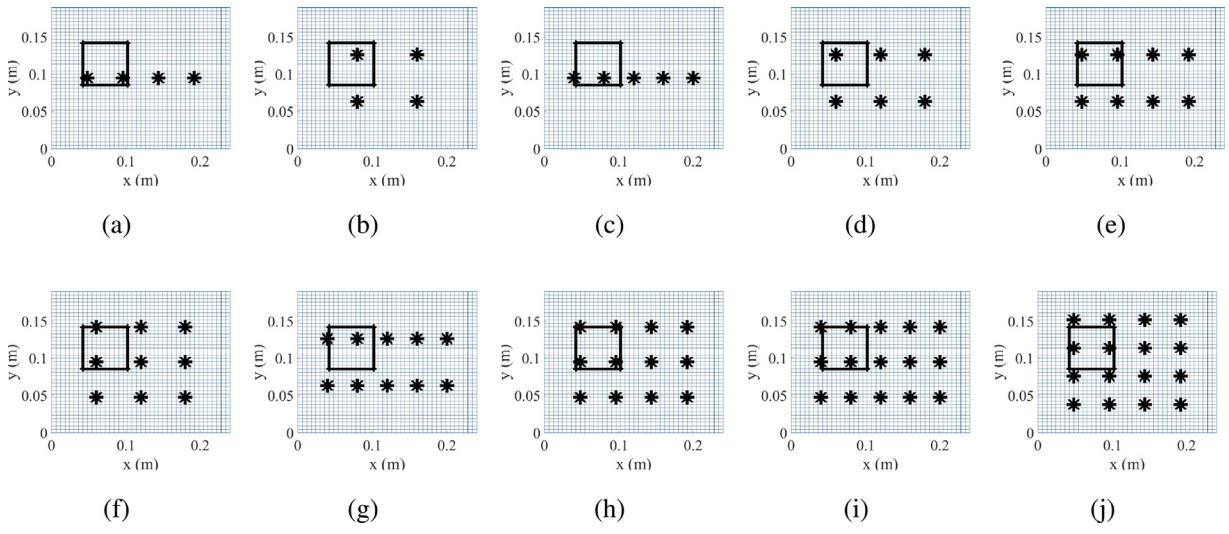

Fig. 4. Disposition of the set of actuators on the plate, and the target shape at ($0.25L_x$, $0.3L_y$).

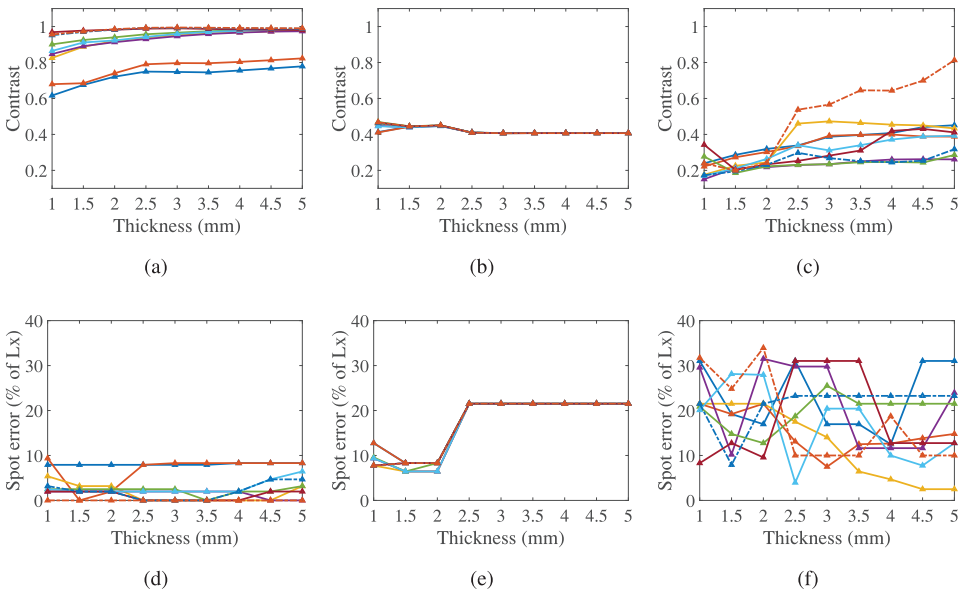

Fig. 5. Contrast and spot error ((a)(d) STIF, (b)(e) TR, and (c)(f) MC) according to the actuator number and disposition, respectively : (4(4 × 1)) (5(5 × 1)) (6(3 × 2)) (8(4 × 2)) (9(3 × 3)) (10(5 × 2)) (12(4 × 3)) (15(5 × 3)) (16(4 × 4))).

According to the Fig. 5a, for the STIF method, increasing the number of actuators allows to increase contrast and to diminish the spot error, whatever the thickness. Indeed, for the two configurations where there is only a line along x, the contrast goes from 0.6 to 0.8. Moreover, when the configuration has at least two lines of actuator, the contrast is comprised between 0.8 to 1. This result can be explained by the fact that more information is available during the learning step. Conversely, for the TR, there is better localization between 1 mm and 2 mm of thickness. For these thickness values, there are better results when the number of actuators increases, because there is more information available in the propagator operation. In addition, in the case of modal control, the contrast increase in general with the width of each configuration. Particularly, from 3mm, the spot error of the configuration (3 × 2) decreases drastically from 10% to 3%, and the contrast is around 0.5. Therefore, the target shape is well located but with some small amplitudes around which increases the contrast. Additionally, the configuration (4 × 4) exhibits the highest contrast, that is 0.6 to 0.8 from 2.5 mm until 5mm. This is because the number of controlled modes is 16, which increases the accuracy of the method in the reduced frequency band [100 Hz;800 Hz]. In conclusion, the STIF method increases localization abilities with more actuators, the TR method is almost not influenced by the number of actuators, and the MC method depends highly on the actuator configuration.

4.3.3. Effect of the target shapes position and size

Target shape position

This subsection allows to study the size and the position of the target shape. Considering the results shown Section 4.3.2 and the small number of actuators due to practical limitations, the actuator disposition used here is the (3 × 2). The target shape extension here is also ($0.3L_x$, $0.6L_y$) and the coordinates of the center are varying from $0.2L_x$ to $0.5L_x$ along the x dimension and $0.5L_y$ to $0.75L_y$ along the y dimension, and can be seen Fig. 6a.

The Fig. 7 exhibits the different contrasts for various damping ratios and thicknesses. The contrast obtained by target shape is always above 7.5 and the spot error always under 10%, therefore, the STIF method is not influenced by the target shape location and is always robust in this case. Conversely, from 2.5, the TR contrast is superior to 0.7 and the spot error inferior to 15% for the configurations (3,4,7,8) where the target shape is centered around the center of the plate. When the target shape gets away from the center of the plate, the results of localization are deteriorated. Furthermore, the configuration (2,3,4) gives the highest contrast for the MC method, above 2.5mm.

Target shape size

Different target shape sizes according to x and y alternatively are compared, as shown in Fig. 6b. The sizes varies from (0.25) to (0.4) according to x and y respectively and is centered at (0.3,0.6). There are totally 16 shapes, more rectangular or square. The main idea is to study the influence of the shape.

The Fig. 8 presents the contrast and spot error for each method according to the thickness and the target shape positions. The STIF method also shows here the best results with a contrast above 7.5 for each position and increasing along the thickness. Moreover, the spot error is also low, always below 10%. This result exhibit the robustness of the method because it can localize for any shapes. Conversely, the TR method shows better results for thicknesses from 1 mm to 2 mm, where the contrast is around 0.5, after it, even if the contrast increases, the spot error also become much higher. Finally, the

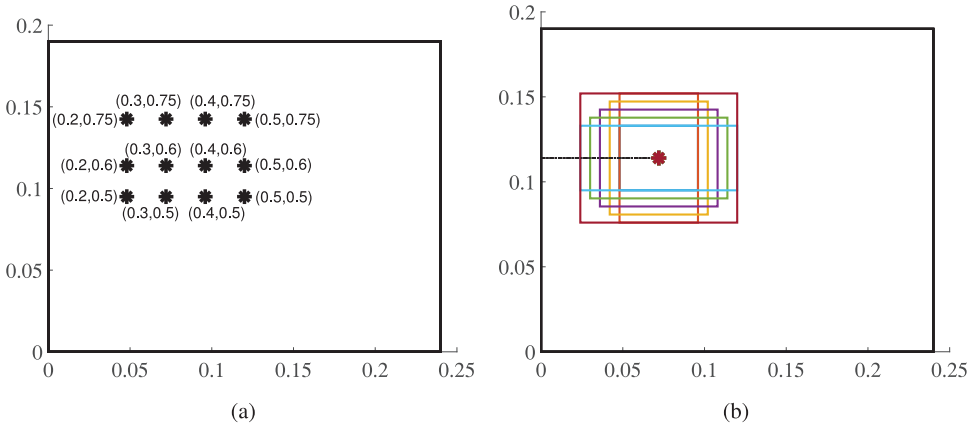

Fig. 6. (a) Positions of the centers and (b) sizes of the target shapes for the parametric study.

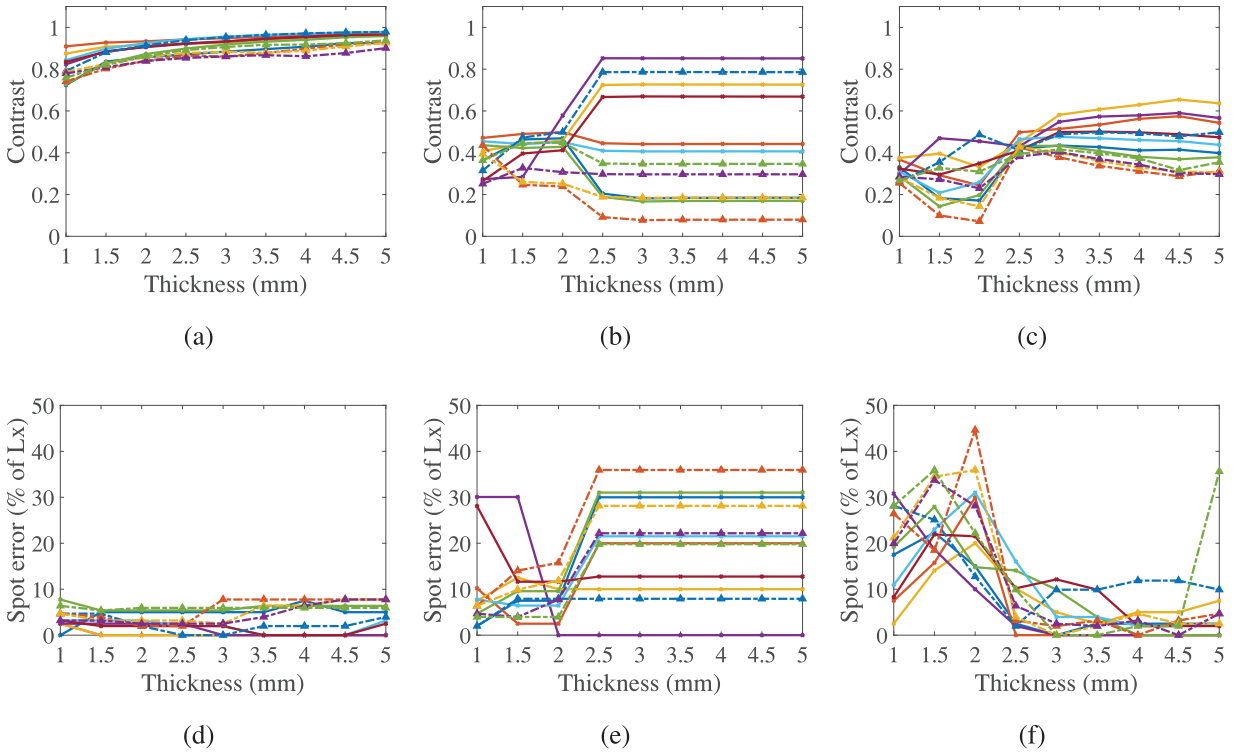

Fig. 7. Contrast and spot error ((a)(d) STIF, (b)(e) TR, and (c)(f) MC) according to the target shape center, respectively at : (1(.2,.5)) (2(.3,.5)) (3(.4,.5)) (4(.5,.5)) (5(.2,.6)) (6(.3,.6)) (7(.4,.6)) (8(.5,.6)) (9(.2,.75)) (10(.3, .75)) (11(.4,.75)) (12(.5,.75)).

contrast for MC is around 0.3 to 0.6, depending on the size. The bigger the size, the more the contrast increases and the spot error diminishes.

4.4. Bending wave focusing detailed examples

4.4.1. Simple structure

In this subsection, an example is detailed in order to illustrate the various method presented in the frequency domain thanks to the parametric study. The target shape and the actuator disposition are provided in Fig. 4d.

The spot error and the contrast in the frequency band [100 Hz;800 Hz] for each method for the simple structure are plotted in Fig. 9. Firstly, we can observe that the STIF method allows achieving a very high localization performance, in comparison with others. Indeed, it shows a very low spot error, which is around 12% of the total length in the [100 Hz;220 Hz] region, and lower than 10% above 220 Hz approximately until 540 Hz (Fig. 9). It is important to notice that this frequency

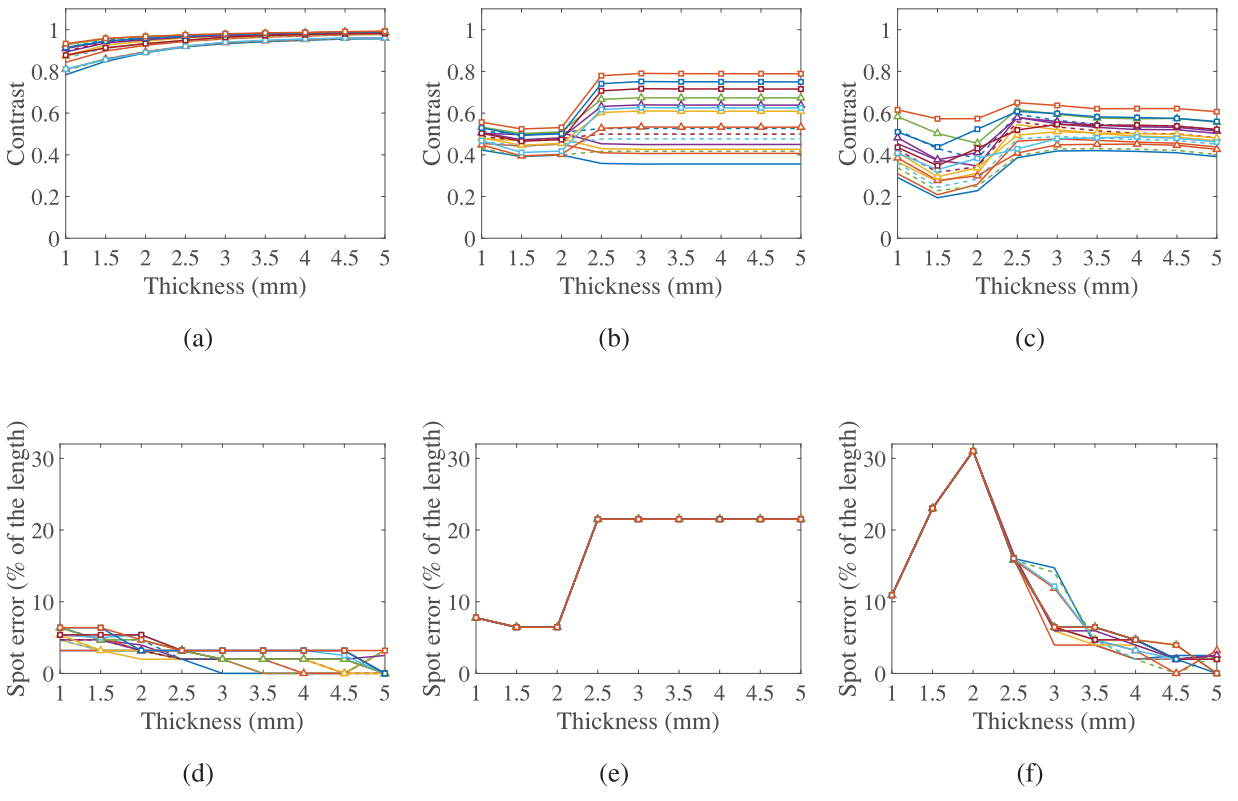

Fig. 8. Contrast and spot error ((a)(d) STIF, (b)(e) TR, and (c)(f) MC) according to the target shape size: (1(.25,.25)) (2(.25,.3)) (3(.25,.35)) (4(.25,.4)) (5(.3,.25)) (6(.3,.3)) (7(.3,.35)) (8(.3,.4)) (9(.35,.25)) (10(.35, .3)) (11(.35,.35)) (12(.35,.4)) (13(.35,.25)) (14(.35, .3)) (15(.35,.35)) (16(.35,.4)).

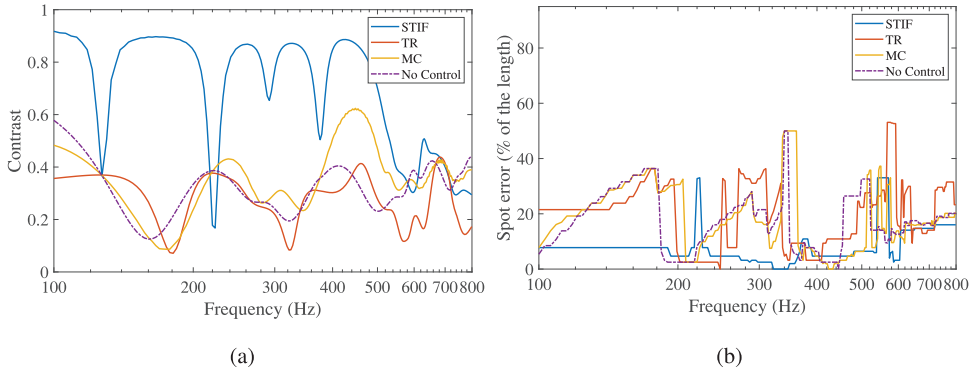

Fig. 9. (a) Spot error and (b) contrast for the simple plate.

corresponds to the limit where the modal density (number of modes/Hz) is very high. Thus, above this frequency the plate could not be described with a modal behavior anymore [7]. Moreover, the contrast drops drastically at modal frequencies, with a peak of the error at 220 Hz and a small around 380 Hz (Fig. 9). It corresponds to the eigenmodes which influences largely the target shape pattern. Indeed, this phenomenon is natural, but can be enhanced by the placement of actuators to increase the controllability of those specific modes. Therefore, the STIF method can achieve a precise localization from 100 Hz to 540 Hz. For higher frequencies, the algorithm does not focus vibrations anymore. It is interesting to notice that there is the same behavior in the frequency band for the MC and for the case without control, also highly influenced by eigenmodes. Besides, according to the spot error and contrast curves, the MC method can focus on the whole frequency band, but more efficient in the bandwidth between 380 Hz and 500 Hz approximately, and with a high influence of the fourth (2,2) mode. However, the no control case is more influenced by the (1,1) mode but does not focus on the whole frequency band. The time reversal (TR) also operates in a narrow band, with a maximal contrast of 0.4, and a very high

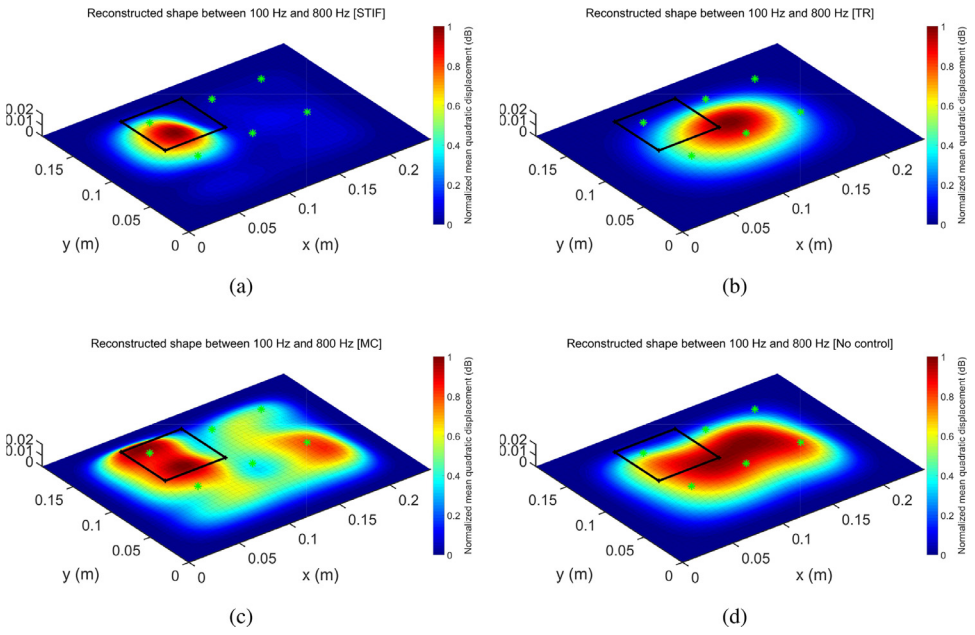

Fig. 10. Reconstructed shapes with (a) STIF, (b) TR, (c) MC and (d) without control.

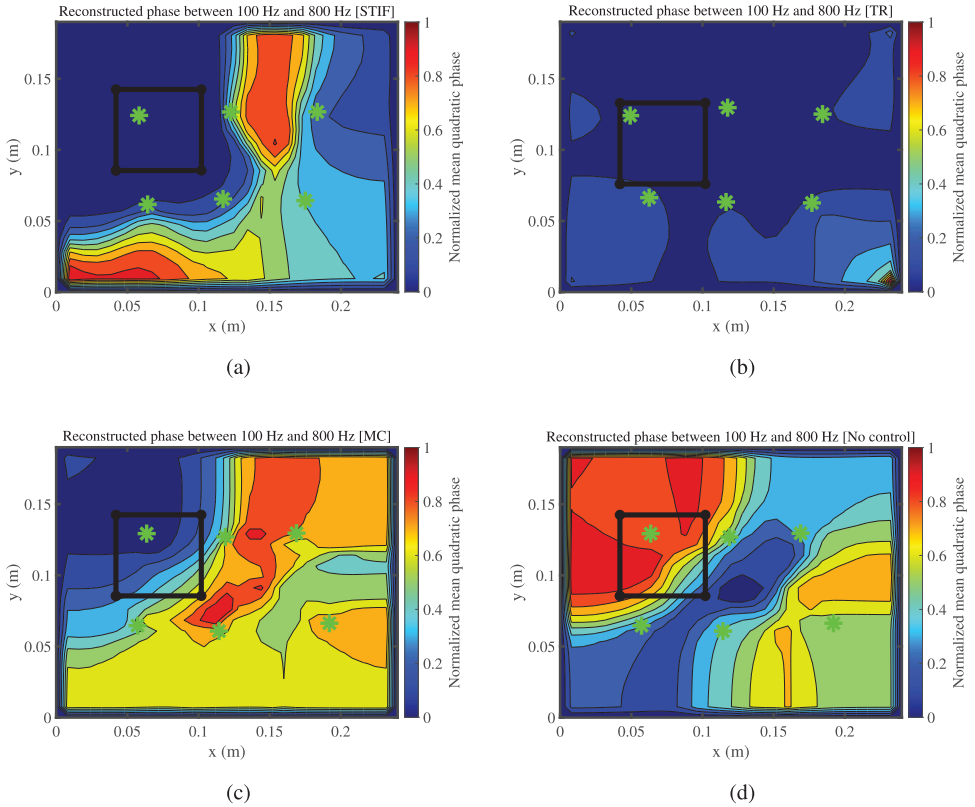

Fig. 11. Reconstructed shape phases with (a) STIF, (b) TR, (c) MC and (d) without control.

influence of the first mode shape which determines the final shape. This is due to the high damping in the material and the high thickness.

An overview of the results of localization obtained in the frequency band of interest is plotted in Fig. 10 through the normalized mean quadratic displacement amplitude and in Fig. 11 through the mean quadratic phase variation. From Fig. 10, it can be seen that the vibration amplitude is on average much more localized by using the STIF method than any other

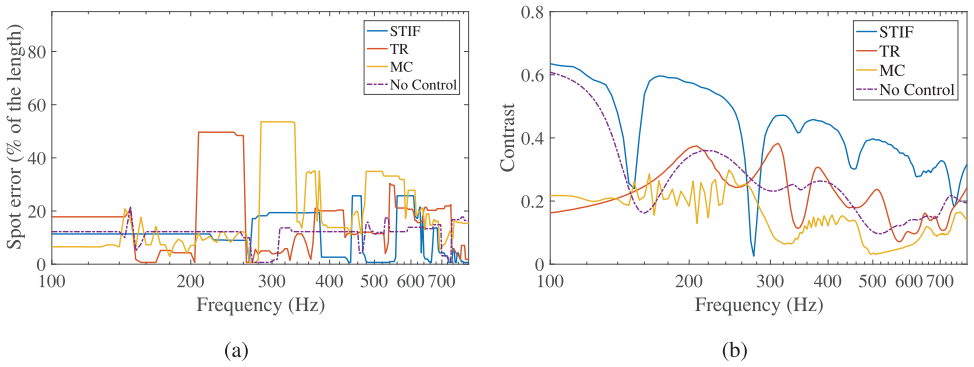

Fig. 12. (a) Spot error and (b) contrast for the plate with ribs.

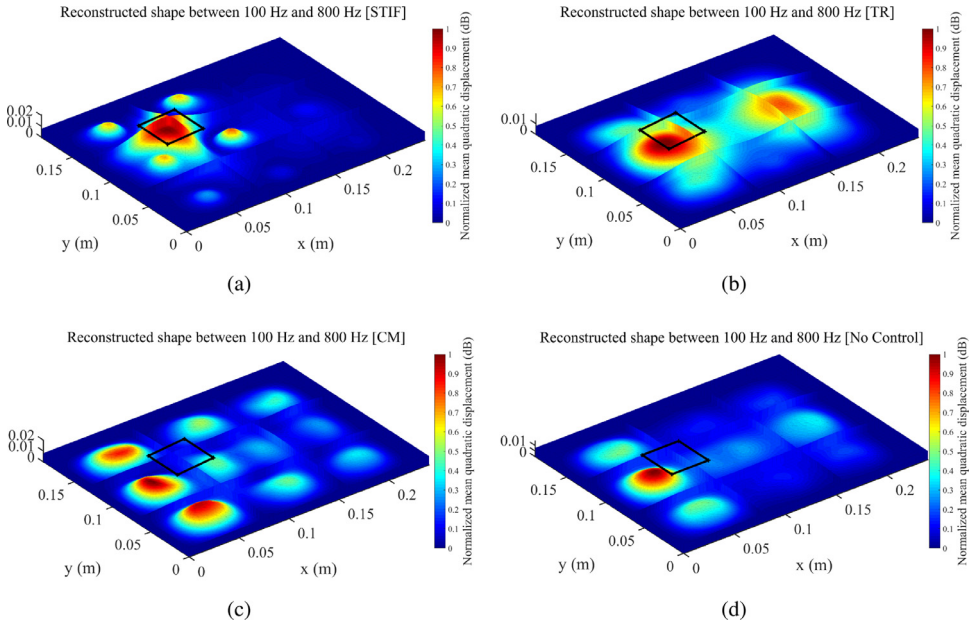

Fig. 13. Reconstructed shapes with (a) STIF, (b) TR, (c) MC and (d) without control.

method. From Fig. 11, it can be concluded that the STIF method additionally guarantees almost no phase variation within the target area, meaning that all the points in that area are vibrating spatially coherently. This is also true in this case for the TR method, true to a lower extent for MC, and not true at all for the no control case.

4.4.2. Effect of the complexity (RIBs)

The studied structure is now the plate as introduced above with ribs fixed on it. The main idea is to see which method will still work on a more complex structure representative of what can be encountered in practical industrial applications. Moreover, the modal frequencies are higher than before, from 154 Hz to 590 Hz, and the modal amplitudes are located between ribs.

The Fig. 12 shows the spot error and the contrast. On the frequency band between 100 Hz and 800 Hz, the STIF method localizes the energy in the target area, similarly to the simple case with 6 actuators (Fig. 13a). Additionally, the contrast drops at frequencies where modes appear. However, the higher values of the error between 270 and 380 Hz correspond to high amplitude vibrations on actuators around the target area but the shape is still reproduced with high contrast. In addition, the TR method can focus the waves in the selected frequency band (Fig. 13b), but it does not maintain the correct target shape for each frequency. Furthermore, the MC method localizes the energy alternatively close to the target shape and between ribs (Fig. 13c), but does not work well since the mode shapes are not conventional flexural modes but a mixture of global and local modes. Finally, without control strategy, the energy is also confined between the ribs near the target shape and shows better precision than MC and TR (Fig. 13d). The initial learning of the dynamic behavior allows having better focusing precision by considering the local modes in the dynamics, in a wider frequency band. When the number of actuators is higher, it increases the localization capabilities.

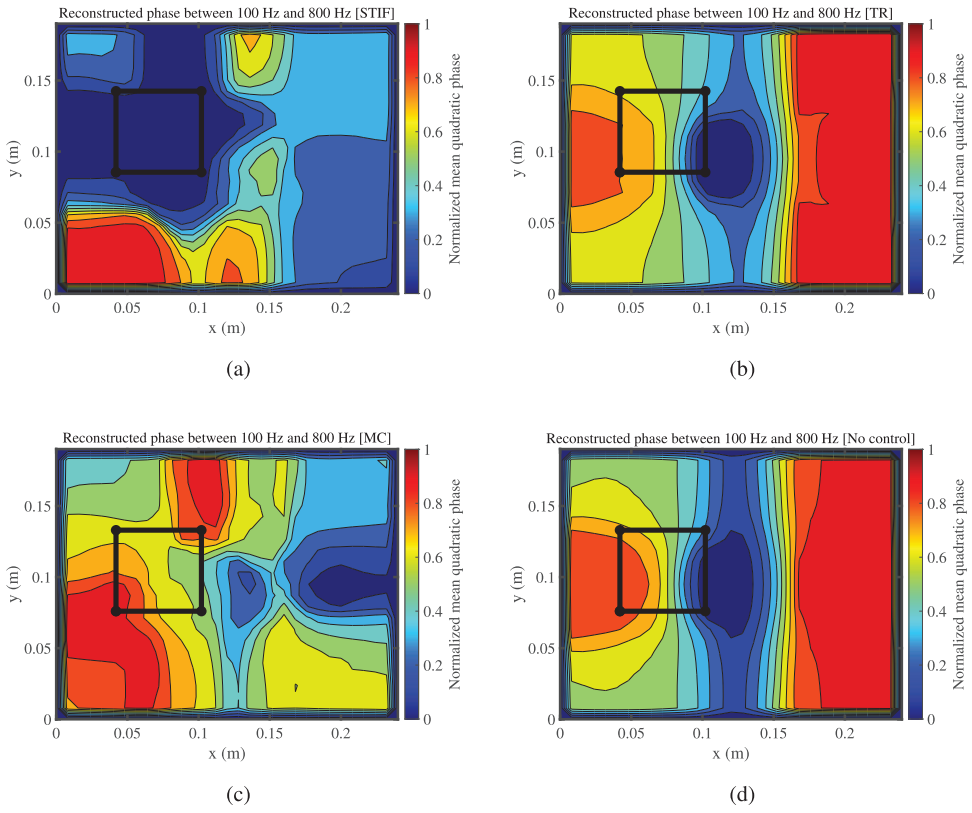

Fig. 14. Reconstructed shape phases with (a) STIF, (b) TR, (c) MC and (d) without control.

Fig. 14 shows the mean quadratic phase variation for the various approaches. It can be seen again that the STIF method guarantees almost no phase variation within the target area, meaning that all the points in that area are vibrating spatially coherently. This is however not anymore true in this case for the TR method, the MC method, and the no control case as they suffer from the presence of the RIB.

4.5. Discussion

4.5.1. About the spatial focusing capabilities of the investigated methods

The previous parametric study allows understanding the influence of damping, thickness, actuator disposition and the target shape for each method. The MC approach is very sensitive to the thickness and damping because it changes the spread of the modes used in the frequency band of interest. Indeed, the larger the number of actuators is, the larger the number of controlled modes will be, and the better the results will be. However, the disposition of actuators is also important for this method because it can excite more specific modes than others if they are placed on a vibration node or anti-node (Fig. 10c). On the other side, the STIF method is based on the learning of the propagation operators between each observation point and actuator. Hence, this method is easier to implement than the MC but requires much more computation time. This means that the STIF allows focusing far better bending waves in the frequency band of interest, as shown in Fig. 10a. Besides, these results allow understanding that the STIF method is always very robust because of the large amount of information known about the propagation operator, thus, the larger the number of actuators the better the algorithms results are. In opposition, the TR method based on a partial knowledge requires less computation time than the STIF, but in this case is less efficient than STIF and gives poorer localization precision (Fig. 10b). Indeed, the TR uses a few information available on actuators, needs to be used in a lightly damped media because it necessitates several reflections on boundaries, therefore on a lightly damped and thin plate. This is a reason why the TR operates better for thinner plates than thicker plates. Finally, when there is no control, the energy is spread around the plate and there is no localization (Fig. 10d). In addition, previous section analyzed energy focusing in the target area as well as the global in phase movement of the target shape for the various investigated methods and the two investigated cases. For the simple case, STIF, TR and MC methods provided adequate and spatially coherent focusing, but for the RIB case, only the STIF method was able to do so.

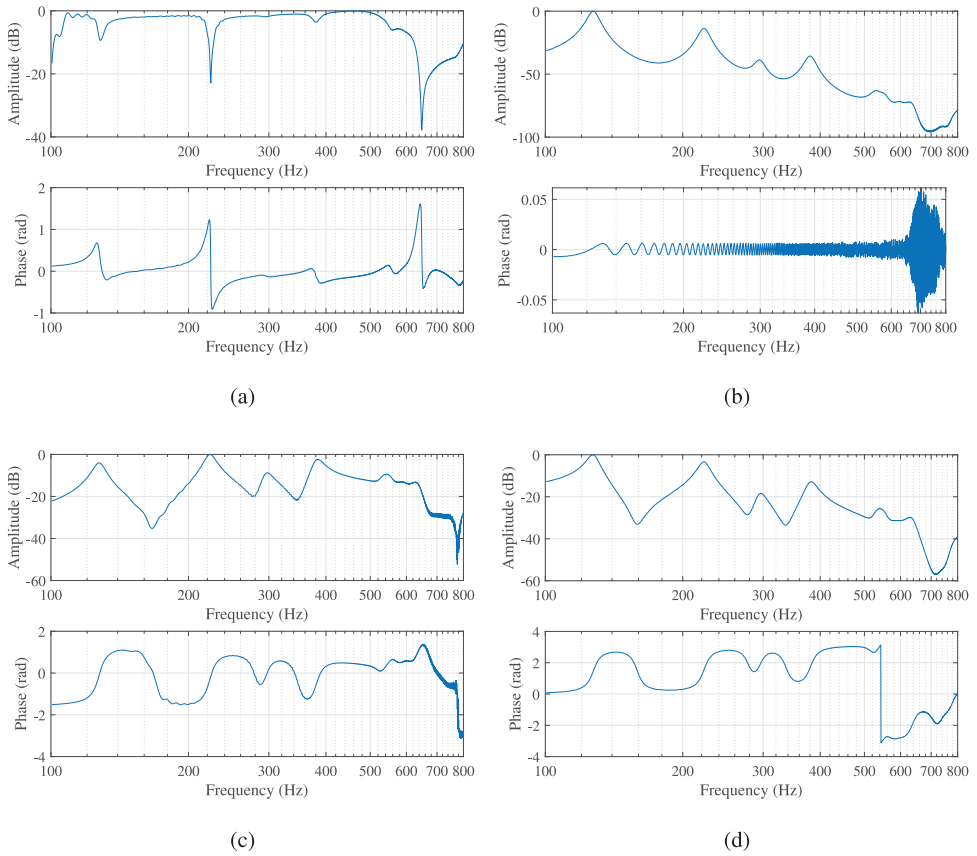

Fig. 15. Frequency response between the input sweep and the center of the target shape maximum vibration, for (a) STIF, (b) TR, (c) MC and (d) No control.

4.5.2. About the temporal focusing capabilities of the investigated methods

After studying the bending wave focusing algorithms in terms of spatial abilities, this subsection illustrates the temporal phase properties associated with the various investigated methods. Indeed, the time domain characteristics of a signal must be precisely controlled for any audio application. In practice, we face here issues similar to the ones faced when using other conventional or panel-based loudspeakers. These issues are associated to i) signal processing, ii) hardware limitations and iii) properties of the material (damping and modal behavior). Therefore, and as for any other audio rendering device, we are not fully reproducing the phase along the whole spectrum but come as close as possible to it. To limit the impact of signal processing related phase distortions, FIR filters which possess linear phase and thus induce only a global and frequency independent delay have been chosen to implement the spatial focusing methods. To limit the impact of hardware related phase distortion, hardware dedicated to audio has been used. And finally, we cannot limit the impact of the vibrating material due to existing modes and have to live with it as it is the case for traditional loudspeakers (membrane modes in the high frequency range) or for panel loudspeakers (panel modes in the low frequency range). In that sense, the proposed approach in thus similar regarding phase issues than any other high-fidelity audio approach and do not introduce any additional phase mismatch as FIR filters have been retained for signal processing.

As all the filtering process and the natural filtering by the host structure are considered here as linear, the waveform of the response in the targeted area is a linearly filtered sweep signal when the considered input is a swept sine excitation. More precisely, according to Eq. (1), all the spatial points within the target area should have a vibration corresponding exactly to this swept sine signal excitation. However, in practice, due to signal processing, hardware limitations, and modal response of the structure that are unavoidable in any audio rendering device (either an electrodynamical loudspeaker or a panel-based one), we are not fully achieving this goal but come as close as possible to it as shown in Fig. 15. This figure represents the amplitude of the frequency response between the sweep input audio signal and the displacement on the point with the maximum amplitude of the target shape for the simple simulated plate. For the STIF, the amplitude of the frequency response is comprised between 0 dB and -2 dB until 500 Hz, where the localization is not anymore correctly achieved as discussed earlier. Furthermore, there are dips that can be observed at the resonance frequencies which shows that the modes are still influencing the whole plate response. In addition, the same figure exhibits the phase after removing the linear trend corresponding to the global delay induced by the FIR filters. The influence of modes is still apparent in the phase response, with phase jumps at resonance frequencies. It is important to notice that in this simulation case, the TR

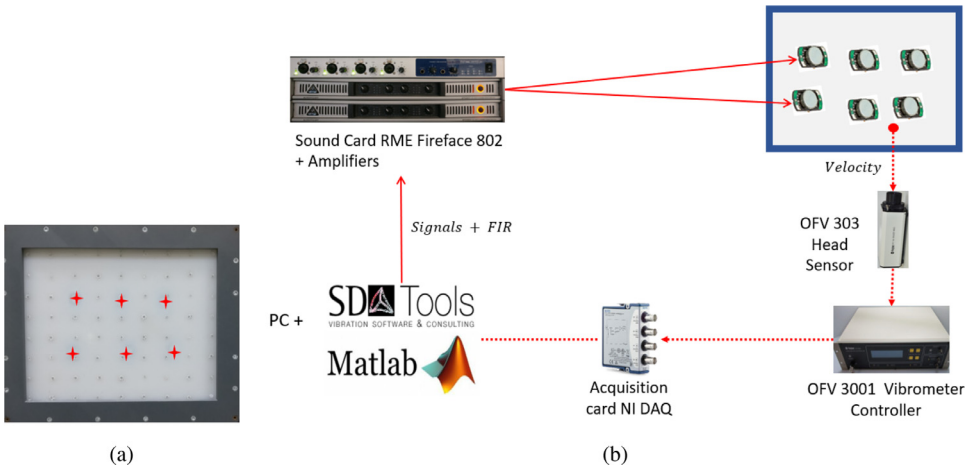

Fig. 16. (a) Plate with actuators position in red and (b) experimental setup used for this study. (For interpretation of the references to colour in this figure legend, the reader is referred to the web version of this article.)

method performs extremely well with respect to temporal phase issues. Finally, compensating for such phase mismatch is something very common in the audio industry and should be managed a posterior through adequate equalization filters.

5. Experimental validation

5.1. Experimental setup

To validate the previous methods, an experimental test campaign was carried out. The tested structure is the polypropylene clamped plate with the same dimensions and properties mentioned before. This material is widely used in the automotive industry as door car panel garnishment. The plate is actuated by six moving coil actuators *TEAX14C02-8* amplified with a *Berhinger EPQ304 Europower* amplifiers and the signals are managed thanks to a *RME Fireface 802* sound card and Matlab also for signals generations. The velocity field of the plate is scanned by a vibrometer comprised of an OFV-303 head scanning head and its OFV-3001 controller, through a *NIDaq USB 9234* acquisition card. The test rig made up of is available in Fig. 16a.

The first step consists in learning the dynamic of the structure. To that end, a first modal experimental analysis was made by exciting the structure. Each exciter is successively actuated with a logarithmic sine sweep from 100 Hz to 2 kHz, during 5s and sampled at 44.1 kHz. The velocity field is acquired by a 72 point grid spanning the plate (Fig. 16b). After the learning step, the frequency response functions are computed, the propagation operator is generated and inverted so that the STIF and TR filters are computed by a routine developed in Matlab according to the process described Section 3.3. Moreover, for the STIF and the TR, the filters obtained above with numerical learning phase will be used to compare the relevance of using a digital twin. Regarding the MC filters, an identification procedure is performed using SDTools Software (results are presented in Table 1) to compute the filters. The target shape size is also $(0.25L_x, 0.3L_y)$, as well as the center located at $(0.3L_x, 0.6L_y)$.

5.2. Experimental validation on a simple plate

5.2.1. Results using experimental data

Firstly, even if the parametric study shown that the larger the number of actuators is the more the algorithms are efficient, we chose to use the minimum possible number of actuators to fit to real conditions. Indeed, the congestion, mass and power supply are several factors forcing to reduce the number of actuators.

Secondly, here, the results are presented as the same format as above with the same configuration made available in Section 4.4.1. The Fig. 17b presents the contrast and spot error of the reconstructed target shape. The Fig. 18 presents the mean quadratic velocity profile of the plate between 100 Hz and 800 Hz. Until 500 Hz, the contrast of the STIF method is above 0.6 and after decreases slightly, except for some frequencies. Indeed, those drops corresponds to mode shapes of the plate and as seen in the numerical example, this method is sensible to mode shapes. Moreover, the spot error is below 15% until 500 Hz except for frequency drops where it increases. After 500 Hz, the method is less efficient, the contrast decreases between 0.2 and 0.5 and the error increases highly. In addition, the contrast obtained by MC oscillates between 0.2 and 0.8 but most of the time is above 0.4. As a consequence, the averaged operative deflection shape between 100 Hz and 800 Hz shows efficient capabilities on focusing. The time reversal doesn't locate the bending waves in this case, because of the highly damped media, the thickness and the low number of actuators. When no control is applied, the maximum of energy

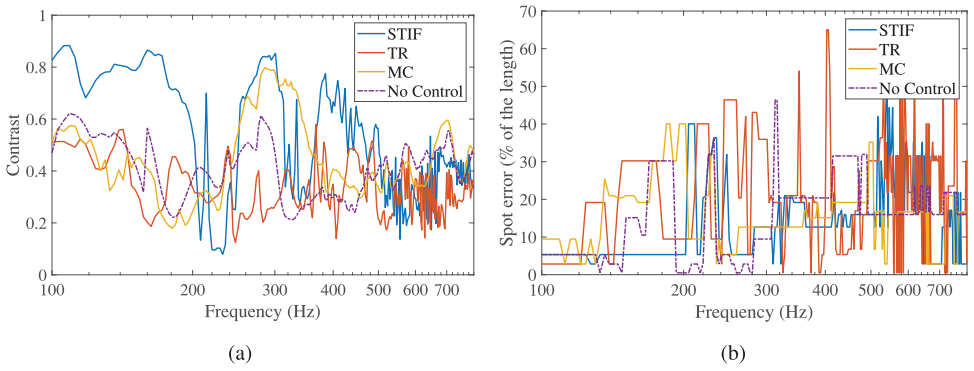

Fig. 17. (a) Contrast and (b) spot error for the experimental study.

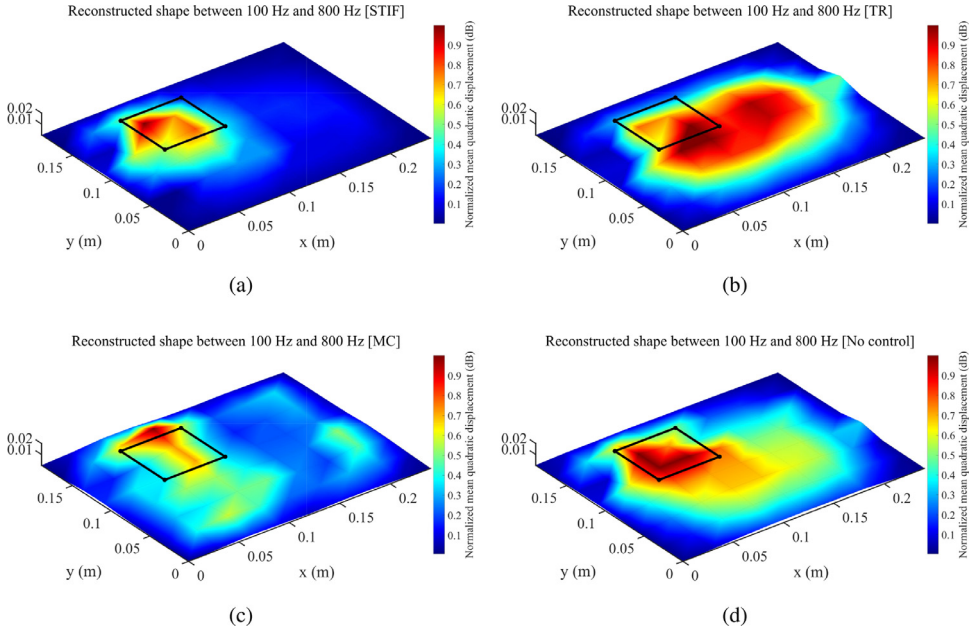

Fig. 18. Experimental reconstructed shapes with (a) STIF, (b) TR, (c) MC and (d) without control.

is localized (mostly until 300 Hz, and after at higher frequencies) around the target shape and thus the actuator even if there is a high amount of energy around (Fig. 18d). The results are very similar to the numerical results presented in Fig. 9. The method is less efficient after 500 Hz for the STIF experimentally as well as numerically. Moreover, there is the same evolution pattern for the three other methods.

5.2.2. Results using a digital twin

This subsection allows to investigate the use of a digital twin instead of learning on a real structure. Indeed, experimental campaigns induce heavy setup preparation, costs a lot of processing time and a large amount of data to post process. Moreover, it introduce bias due to noises. The MC method is not shown here because the filters are computed according to the knowledge of the modal properties, and here, the mode shapes based on analytic model, FEM, and experiment leads to the same filters.

Hence, the Fig. 19 shows the comparison between the previous experimental results and the results obtained by using numerical filters produced by simulation. The STIF contrast is high as for the experimental result until 300 Hz which corresponds to a very typical mode shape. Thereafter, the contrast is comprised between 0.2 and 0.5 after 300 Hz and is approximately the same as experimental STIF after 500 Hz. However, the TR generated experimentally shows a slightly better contrast than the TR generated numerically, but still low compared to other methods. They exhibit as well the same reconstructed shape and contrast pattern as the numerical study before. The velocity profiles in the frequency band of interest are available Fig. 20.

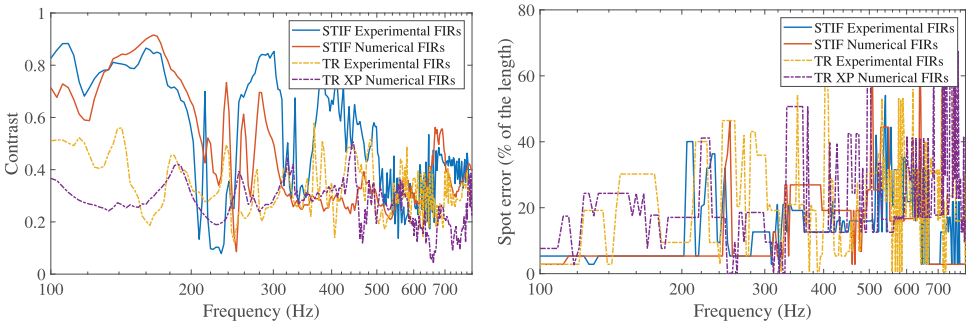

Fig. 19. (a) Contrast and (b) spot error for the numerical vs experimental generated filters for STIF and TR.

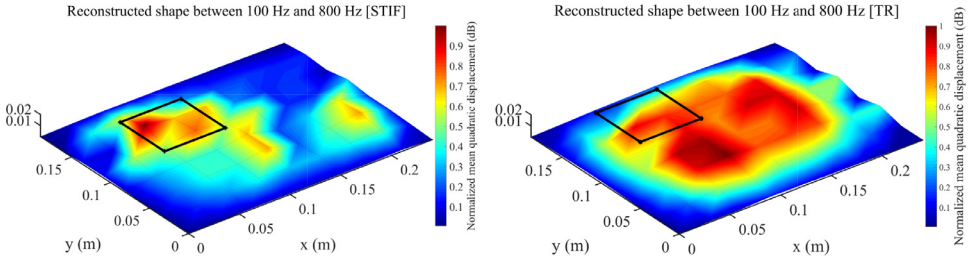

Fig. 20. Experimental reconstructed shapes with numerical generated filters (a) STIF and (b) TR.

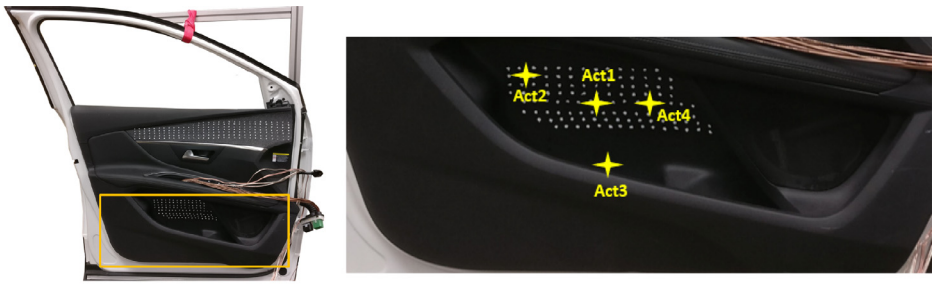

Fig. 21. (a) The door car panel studied (b) and the zone of interest.

The results exhibit the possibility to learn with the numerical model, which can present several benefits mentioned above. Hence, the STIF method is not very sensitive to noise and the finite element model can be translated into the experimental model for the learning step.

5.3. Application on a door car panel

Now, the STIF method is applied on a door car panel to focus vibrations on a specific area allowing to generate low frequencies. Here, 4 *PUI Audio ASX05408-HD-R* electromagnetic actuators are used to focus vibrations, and will allow to avoid the low frequency modal behavior. The same experimental setup is used, with here 102 points stuck on the plate to scan the velocity profile, with the same learning step procedure. The door car panel, the reflective points denoting the sensing area and the actuator location are available Fig. 21. A numerical study on the FEM model shows that there is more than 300 modes in the [20 Hz,200 Hz] frequency band. Thus, the modal density is very high. The TR and MC are not used because of the small number of actuators used here, due to the small area available.

The velocity profile for the actuators driven separately are shown in Fig. 22. Moreover, the Fig. 23 shows the velocity profile of the reconstructed shape thanks to the STIF method between 100 Hz and 500 Hz. The method can thus localize the vibrations between actuators quite accurately to control the shape of the door car panel and increase the sound reproduction capabilities.

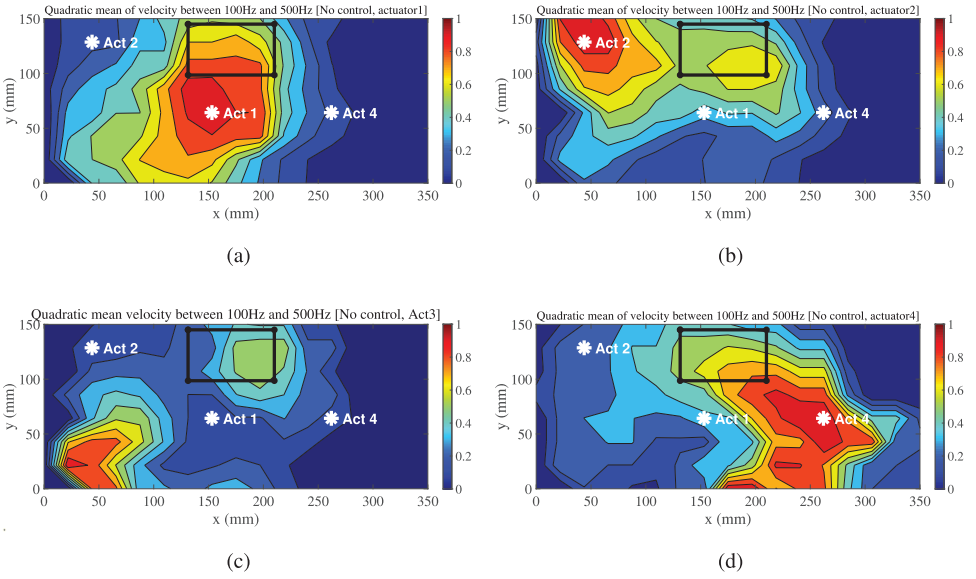

Fig. 22. Experimental reconstructed shapes with only (a) actuator 1, (b) actuator 2, (c) actuator 3 and (d) actuator 4 active.

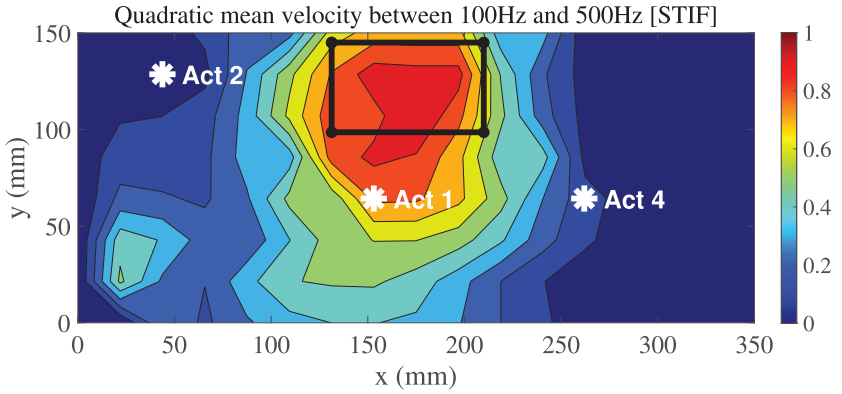

Fig. 23. Experimental reconstructed shape with the STIF method.

6. Conclusion

To conclude, three focusing wave methods were tested and adapted for bending waves in the case of sound reproduction. Firstly, there were compared according to a numerical model, and after validated on an experimental case. Also, the STIF was reproduced on a door car panel and shows very good results at low and high frequencies, where the vibrations stay located around the actuator. Within the context of automotive industry and spatial sound rendering, it is obvious that the spatio-temporal inverse filtering method is easier to implement and gives better results compared to others, even on a complex structure. Indeed, the filters are computed without prior knowledge about boundaries or theoretical dynamic behavior. However, the computation cost is higher, because the structure dynamic must be learned before. In contrast, it was shown that the learning step can be made thanks to a digital twin and gives in this case very good results. Above a certain frequency where the methods focus poorly, only exciting the actuator located near the target shape would be enough. Mainly for highly damped structures and at high frequencies. Finally, several parameters as the modal density, the number of actuators and the characteristics of the target shape have been studied as they influence on the localization results. Those parameters must be taken into account, regardless of the complexity of the structure. As a consequence, some prospects flowing from this work can be underlined. Firstly, the comparison of those methods and the drawbacks associated will allow considering active control to increase the robustness in case of complex structures and subjected to several perturbations (operational conditions...). Secondly, the use of digital twins will allow to ease the study of complex structures and learning phases. This will serve to enhance the industrialization of this kind of technology in automotive industry.

Declaration of Competing Interest

The authors declare that they have no known competing financial interests or personal relationships that could have appeared to influence the work reported in this paper.

CRediT authorship contribution statement

Nassim Benbara: Methodology, Software, Validation, Writing - original draft. **Marc Rebillat:** Conceptualization, Methodology, Software, Supervision, Writing - review & editing. **Nazih Mechbal:** Funding acquisition, Supervision, Writing - review & editing.

Acknowledgments

This work was financially supported by the French National Research Agency (ANR, contract ANR-17-CE33-0004). The authors wish to thank Christian Bolzmacher from CEA and Jean-Christophe Chamard from PSA for their help in providing the car and some hardware for experiments.

References

[1] A.J. Berkhout, D. de Vries, P. Vogel, Acoustic control by wave field synthesis, J. Acoust. Soc. Am. 93 (5) (1993) 2764–2778, doi:10.1121/1.405852.
[2] R. Rabenstein, S. Spors, Spatial aliasing artifacts produced by linear and circular loudspeaker arrays used for wave field synthesis, Audio Engineering Society Convention 120, 2006. http://www.aes.org/e-lib/browse.cfm?elib=13515.
[3] N. Harris, M.J. Hawksford, The distributed-mode loudspeaker (DML) as a broad-band acoustic radiator, Audio Engineering Society Convention 103, 1997. http://www.aes.org/e-lib/browse.cfm?elib=7253.
[4] M.M. Boone, W.P.J. de Bruijn, On the applicability of distributed mode loudspeaker panels for wave field synthesis-based sound reproduction, Audio Engineering Society Convention 108, 2000. http://www.aes.org/e-lib/browse.cfm?elib=9173.
[5] U. Horbach, D. de Vries, E. Corteel, Spatial audio reproduction using distributed mode loudspeaker arrays, in: Audio Engineering Society Conference: 21st International Conference: Architectural Acoustics and Sound Reinforcement, 2002. http://www.aes.org/e-lib/browse.cfm?elib=11196.
[6] M. Kuster, D. De Vries, D. Beer, S. Brix, Structural and acoustic analysis of multiactuator panels, J. Audio Eng. Soc 54 (11) (2006) 1065–1076. http://www.aes.org/e-lib/browse.cfm?elib=13887.
[7] M. Rébillat, Vibrations of large multi-actuator panels for the creation of audio-visual virtual environments: acoustical, mechanical and perceptual approaches, Ecole Polytechnique X, 2011 Theses. https://pastel.archives-ouvertes.fr/pastel-00657634.
[8] J. Escolano, J.J. Lpez, B. Pueo, G. Ramos, On large multiactuator panels for wave field synthesis applications, Audio Engineering Society Convention 124, 2008. http://www.aes.org/e-lib/browse.cfm?elib=14584.
[9] B. Pueo, J.J. Lpez, J. Escolano, L. Hŋrchens, Multiactuator panels for wave field synthesis: Evolution and present developments, J. Audio Eng. Soc 58 (12) (2011) 1045–1063. http://www.aes.org/e-lib/browse.cfm?elib=15745.
[10] A. Preumont, Vibration Control of Active Structures: An Introduction, Solid Mechanics and Its Applications, Springer Netherlands, 2011. https://books.google.fr/books?id=MUQUQyB4bEUC.
[11] E. Enferad, C. giraud audine, G. FrĖdĖric, M. Amberg, B. Semail, Generating controlled localized stimulations on haptic displays by modal superimposition, J. Sound Vib. 449 (2019), doi:10.1016/j.jsv.2019.02.039.
[12] J.-H. Woo, J.-G. Ih, Vibration rendering on a thin plate with actuator array at the periphery, J. Sound. Vib. 349 (2015) 150–162, doi:10.1016/j.jsv.2015.03.031.
[13] M.C. Heilemann, D. Anderson, M.F. Bocko, Sound-source localization on flat-panel loudspeakers, J. Audio Eng. Soc 65 (3) (2017) 168–177. http://www.aes.org/e-lib/browse.cfm?elib=18552.
[14] M. Fink, Time reversal of ultrasonic fields. i. basic principles, IEEE Trans. Ultrason. Ferroelectr. Freq. Control 39 (5) (1992) 555–566, doi:10.1109/58.156174.
[15] M. Fink, C. Prada, Acoustic time-reversal mirrors, Inverse Problems 17 (1) (2001) R1. http://stacks.iop.org/0266-5611/17/i=1/a=201.
[16] S. Yon, M. Tanter, M. Fink, Sound focusing in rooms: the time-reversal approach, J. Acoust. Soc. Am. 113 (3) (2003) 1533–1543, doi:10.1121/1.1543587.
[17] C. Hudin, J. Lozada, V. Hayward, Localized tactile feedback on a transparent surface through time-reversal wave focusing, IEEE Trans. Haptics 8 (2) (2015) 188–198, doi:10.1109/TOH.2015.2411267.
[18] Y. Kahana, P.A. Nelson, O. Kirkeby, H. Hamada, A multiple microphone recording technique for the generation of virtual acoustic images, J. Acoust. Soc. Am. 105 (3) (1999) 1503–1516, doi:10.1121/1.426690.
[19] M. Tanter, J.-L. Thomas, M. Fink, Time reversal and the inverse filter, J. Acoust. Soc. Am. 108 (1) (2000) 223–234, doi:10.1121/1.429459.
[20] M. Tanter, J.-F. Aubry, J. Gerber, J.-L. Thomas, M. Fink, Optimal focusing by spatio-temporal inverse filter. I. Basic principles, J. Acoust. Soc. Am. 110 (1) (2001) 37–47, doi:10.1121/1.1377051.
[21] J.-F. Aubry, M. Tanter, J. Gerber, J.-L. Thomas, M. Fink, Optimal focusing by spatio-temporal inverse filter. ii. experiments. application to focusing through absorbing and reverberating media, J. Acoust. Soc. Am. 110 (1) (2001) 48–58, doi:10.1121/1.1377052.
[22] S. Yon, M. Tanter, M. Fink, Sound focusing in rooms. ii. the spatio-temporal inverse filter, J. Acoust. Soc. Am. 114 (6) (2003) 3044–3052, doi:10.1121/1.1628247.
[23] J.-H. Woo, J.-G. Ih, Y. Park, Comparison of two vibro-acoustic inverse methods to radiate a uniform sound field from a plate, J. Sound Vib. 458 (2019) 445–457, doi:10.1016/j.jsv.2019.06.031.
[24] J. Woo, J. Ih, Generation of a virtual speaker and baffle on a thin plate controlled by an actuator array at the boundary, IEEE/ASME Trans. Mechatron. 24 (3) (2019) 1197–1207, doi:10.1109/TMECH.2019.2906376.
[25] Structural Dynamics Toolbox (for use with MALTAB)], SDTools, Paris, France, https://www.sdtools.com/, Sep 1995–2019.